Journal of Nuclear Materials 444 (2014) 14–22

Contents lists available at ScienceDirect

Journal of Nuclear Materials

journal homepage: www.elsevier.com/locate/jnucmat

In situ monitored in-pile creep testing of zirconium alloys

R.W. Kozar *, A.W. Jaworski, T.W. Webb, R.W. Smith

Bettis Atomic Power Laboratory, West Mifflin, PA 15122, United States

HIGHLIGHTS

- Models compared to in situ monitored in-pile creep data for Zircaloy-2.
- In situ monitoring allowed cover of wide design space with 12 specimens.
- Nichols irradiation creep model best model for predicting steady-state creep rates.
- Dislocation primary creep controlling following change to different test conditions.

ARTICLE INFO

Article history:
Received 3 July 2013
Accepted 24 August 2013
Available online 31 August 2013

ABSTRACT

The experiments described herein were designed to investigate the detailed irradiation creep behavior of zirconium based alloys in the HALDEN Reactor spectrum. The HALDEN Test Reactor has the unique capability to control both applied stress and temperature independently and externally for each specimen while the specimen is in-reactor and under fast neutron flux. The ability to monitor in situ the creep rates following a stress and temperature change made possible the characterization of creep behavior over a wide stress–strain-rate–temperature design space for two model experimental heats, Zircaloy-2 and Zircaloy-2 + 1 wt%Nb, with only 12 test specimens in a 100-day in-pile creep test program. Zircaloy-2 specimens with and without 1 wt% Nb additions were tested at irradiation temperatures of 561 K and 616 K and stresses ranging from 69 MPa to 455 MPa. Various steady state creep models were evaluated against the experimental results. The irradiation creep model proposed by Nichols that separates creep behavior into low, intermediate, and high stress regimes was the best model for predicting steady-state creep rates. Dislocation-based primary creep, rather than diffusion-based transient irradiation creep, was identified as the mechanism controlling deformation during the transitional period of evolving creep rate following a step change to different test conditions.

1. Introduction

Zirconium alloys are commonly used in the nuclear industry as core components due to their low neutron cross-section. Zircaloy-2 and Zircaloy-4 which contain Sn, Fe, and Cr additions have been used as fuel cladding materials since the early days of boiling water reactors (BWR) and pressurized water reactors (PWR). More recently, advanced Nb containing zirconium alloys have been developed as fuel cladding materials. Some commercial examples of Nb containing zirconium alloys are Zr–2.5 wt%Nb, ZIRLO, MDA, E-110, and M5 [1–5].

Despite the widespread use of zirconium alloys in nuclear applications, relatively little in-reactor creep data exists for these materials. Typically, in-reactor creep specimens are periodically removed from a test reactor during an in-pile creep experiment so that measurements of dimensional changes can be recorded. The practical constraints of reactor operating schedules and the need to remove specimens from the reactor to measure dimensional changes greatly complicates the design of optimized test programs and there is substantial risk of missing or losing key data, such as details of transient creep behavior.

Many of the inefficiencies and uncertainties inherent in the design and operation of irradiation creep testing can be eliminated if the mechanical behavior of the samples is monitored in situ and the environmental conditions of the test controlled continuously during irradiation, as is possible in the HALDEN Reactor. The HALDEN Test Reactor, which is operated by the Institutt for Energiteknikk in Halden, Norway, has the unique capability to control both stress and temperature independently and externally for each specimen while the specimen is in-reactor and under fast neutron flux. Additionally, strain data can be monitored in real time using a calibrated linear voltage displacement transducer (LVDT).

The ability to monitor creep strain during irradiation allows one to quickly verify that target strain-rates are being achieved, and to

* Corresponding author. Address: PO Box 79, West Mifflin, PA 15122, United States. Tel.: +1 412 476 3935; fax: +1 412 476 5779.
E-mail address: rwkozar88@yahoo.com (R.W. Kozar).

0022-3115/$ - see front matter © 2013 Elsevier B.V. All rights reserved.
http://dx.doi.org/10.1016/j.jnucmat.2013.08.043

easily distinguish between transient and steady-state modes of deformation. The ability to control both temperature and load in response to real-time feedback allows a much broader range of variables to be sampled with a minimal number of specimens. In situ temperature and stress control also allows investigation of the transient response of a specimen following a stress and/or temperature change. In addition to the benefits with respect to both data collection methods and experimental control, the need for expensive and time-consuming handling of irradiated materials at multiple inspection interims is completely eliminated.

2. Materials and methods

2.1. Materials

Zircaloy-2 and Zircaloy-2 + 1 wt% Nb in a recrystallization annealed (RXA) condition were tested to isolate the effect of Nb addition on the irradiation creep response without the compounding effect of cold-work strains. Both materials were subjected to identical hot rolling, warm sizing, and annealing operations in order to achieve a fully recrystallized microstructure. The chemistry for the Zircaloy-2 and Zircaloy-2 + 1 wt% Nb materials are listed in Table 1 and compared to typical chemical compositions of ZIRLO [2], MDA [3], E-110 [4], and M5 [5].

The Zircaloy-2 material had an equiaxed microstructure with an average grain size of about 25 μm and a Kearns texture factor of 0.59 normal to the rolling direction. The Zircaloy-2 + 1 wt% Nb had slightly elongated grains with a similar average grain size and a Kearns texture factor of 0.45 normal to the rolling direction. The Zircaloy-2 + 1 wt% Nb material included a retained beta Zr (–Nb) phase along grain boundaries which acted to slightly increase its non-irradiated strength relative to the Zircaloy-2 material.

Table 1
Chemical compositions of the Zircaloy-2 and Zircaloy-2 + 1 wt% Nb materials and typical chemical compositions of ZIRLO [2], MDA [3], E-110 [4], and M5 [5].

	Sn	Nb	Fe	Cr	Ni	O	Zr
Zr-2	1.50	0.00	0.15	0.11	0.06	0.15	Bal
Zr-2 + 1Nb	1.45	1.00	0.13	0.08	0.06	0.12	Bal
ZIRLO	1.00	1.00	0.10	–	–		Bal
MDA	0.80	0.50	0.20	0.10	–		Bal
E110	–	1.00	0.014	<0.003	0.0035	0.06	Bal
M5	–	1.00	0.01	–	–	0.01	Bal

Specimens were machined with the tensile axis parallel to the rolling direction of the plate with cylindrical gage sections per HALDEN drawings that complement HALDEN Reactor irradiation capsule designs. Final machined specimens had a gauge length of 56 mm and gauge width of 2.58 mm. Fig. 1 depicts a typical specimen following in-pile creep testing.

2.2. Equipment

The unique capsule load application and control system allowed for load changes to specimens individually and independently. The HALDEN Test Reactor used external pressurization to apply pressure to the bellows which in turn imparted a uniaxial tensile load to the creep specimens. The pressure, thus the load, was independently controlled for each specimen. Specimens were contained in dry capsules filled with a helium–argon gas mixture. Temperature was controlled by manipulating the helium–argon gas mixture within the capsule. Fig. 2 shows a diagram of a HALDEN irradiation capsule specimen holder showing the placement of the test specimen, the bellows used to apply load, and the LVDT which monitored strain measurements.

2.3. HALDEN fluence-to-DPA conversion

Calculation of the displacement damage per unit neutron fluence (DPA per n/cm^2 ($E > 1$ MeV)) was performed using a 190 group energy spectrum file produced with ZENITH and provided by HALDEN [6]. The displacement damage cross section for elemental zirconium was taken from the SPECTER code package [7] and integrated (summed) over this spectrum. Total DPA per unit fast fluence was determined to be 1.52×10^{-21} DPA per n/cm^2 ($E > 1$ MeV). A displacement threshold of 40 eV was assumed.

3. Experimental

Twelve specimens were creep tested at irradiation temperatures of 561 K or 616 K and stresses ranging from 69 MPa to 455 MPa during a 100-day irradiation creep test program. To achieve an initial increment of irradiation hardening prior to creep testing, specimens were pre-dosed without an applied load for 95 days to an approximate fluence of 1.5×10^{20} n/cm^2 ($E > 1$ MeV) under a constant fast neutron flux of approximately

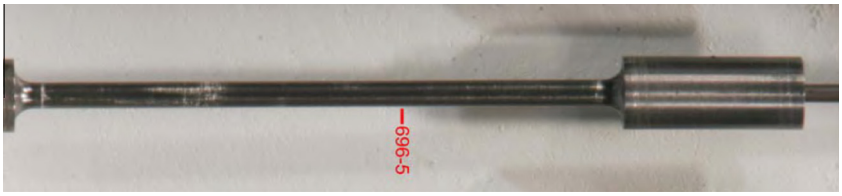

Fig. 1. Picture of Specimen 696-5 after irradiation creep testing.

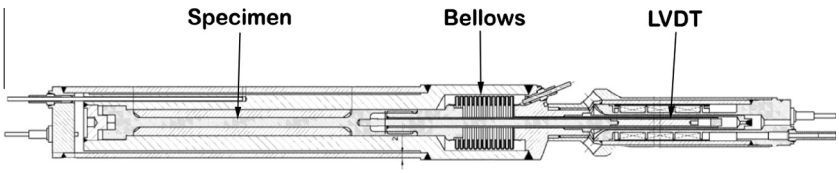

Fig. 2. Diagram of HALDEN irradiation capsule specimen holder showing the placement of the test specimen, bellows which apply load, and LVDT to record strain measurements.

2×10^{13} n/cm^2 s ($E > 1$ MeV). Individual constant loads were applied to each of the 12 specimens that resulted in initial stresses ranging from 69 MPa to 241 MPa, as summarized in Table 2.

Midway into the 100-day irradiation creep experiment, specimens were subjected to changes in applied stress and in one case, test temperature (summarized in Table 2). Stress and temperature changes were conducted to produce additional information about the primary and transient creep responses and allowed for maximized coverage of the stress–creep strain-rate design space. The HALDEN Reactor Project applied stress changes to specimens one at a time while monitoring strain data in real time using a calibrated LVDT. Strain measurements were recorded in 15-min intervals during the entire in-reactor period. In addition to stress changes, the in-pile test temperature of Specimen 696-10 was increased from 561 K to 616 K at constant load on day 55 of the creep experiment. Additional stress transients were applied to six specimens shortly before the conclusion of creep testing on day 92. Specimens 696-7 and 696-9 experienced LVDT failures 49 days into the test program and subsequently did not provide any experimental data.

An additional 12 specimens were irradiated stress-free for the purpose of obtaining out-of-reactor post-irradiated tensile properties and to distinguish creep from stress-free growth. Of these specimens irradiated stress-free, four were removed from the reactor following the 95-day pre-dose cycle to obtain tensile properties of the materials at the start of creep testing. Eight unstressed specimens remained in-reactor for the duration of creep testing to obtain tensile properties of the materials at the conclusion of creep testing.

Table 2
In-pile creep test matrix for specimens, including stress and temperature transients.

ID	Material	Temp. (K)	Stress (MPa)	Day of transient
696-1	Zr-2	561	138	Initial
			310	51
			352	56
696-2	Zr-2 + 1Nb	561	241	Initial
			365	55
			400	56
			427	92
696-3	Zr-2	561	241	Initial
			331	52
696-4	Zr-2	616	138	Initial
			276	55
696-5	Zr-2 + 1Nb	616	172	Initial
			310	57
			372	92
696-6	Zr-2	616	69	Initial
			248	56
			303	92
696-7	Zr-2	616	172	Initial
			LVDT Failed @ Day 49	
696-8	Zr-2 + 1Nb	616	103	Initial
			331	56
			352	92
696-9	Zr-2	616	103	Initial
			LVDT Failed @ Day 49	
696-10	Zr-2	561	172	Initial
		Temp. transient to 616 K @ Day 55		
		Stress transient to 290 MPa @ Day 92		
696-14	Zr-2 + 1Nb	561	172	Initial
			400	57
			455	92
696-12	Zr-2	561	172	Initial
			372	57

Tensile testing of these 12 irradiated stress-free specimens was conducted at the Institutt for Energiteknikk in Kjeller, Norway. The four specimens that were removed from the reactor following the 95-day pre-dose cycle were tensile tested at their in-pile irradiation temperatures of 561 K or 616 K. Four specimens that were irradiated for the entire creep program were also tested at their in-pile irradiation temperatures of 561 K and 616 K. Additionally, four specimens irradiated unstressed for the entire creep test program were tensile tested at room-temperature. The test matrix for tensile testing of stress-free specimens irradiated in the HALDEN Test Reactor is included as Table 3.

4. Results

4.1. Steady-state creep

Experimentally measured minimum strain-rates for the Zircaloy-2 and Zircaloy-2 + 1 wt% Nb specimens are included in Table 4. Specimens that were subjected to multiple sets of test conditions include strain-rates listed for each set of test conditions. A true minimum (steady-state) creep rate as defined by a minima on a log (true strain-rate) vs. log (true plastic strain) was only observed for four of the thirty sets of test conditions (Fig. 3). Study of the log (true strain-rate) vs. log (true plastic strain) plots indicated that the majority of the specimens were nearing a steady-state creep rate, with the notable exception being the second set of test conditions for Specimen 696-2. The log (true strain-rate) vs. log (true plastic strain) plots also indicated that the initial 50–57 day stressed irradiation creep period was insufficient to estimate steady-state creep rate at the lowest stress for each specimen since accumulated strains were low. Minimum creep rates reported in Table 4 represent the minimum creep rate observed for a specimen at a given set of test conditions.

4.2. Primary creep

Fig. 4 shows an in-pile creep curve for Specimen 696-2 irradiated at a nominal temperature 561 K and a fast neutron flux of 2×10^{13} n/cm^2 s. This specimen was irradiated in-pile at an applied stress of 243 MPa for 55 days before being subjected to three additional planned stress step-changes. At the beginning of the test and after each load change, a period of changing creep rate is observed.

Throughout the irradiation creep program there were periodic reactor shutdowns, both planned and unplanned. Fig. 4 indicates periods of reactor shutdown in hours. After the longest shutdown, occurring after 49 days of in-pile creep, the specimen took several

Table 3
Test matrix for tensile testing of stress-free specimens irradiated in the HALDEN Reactor.

ID	Material	Flux (n/cm^2 s)	Fluence (n/cm^2)	Irradiation temp. (K)	Test temp. (K)
696-15	Zr-2	2.02×10^{13}	3.8×10^{20}	561	561
696-16	Zr-2 + 1Nb	2.04×10^{13}	3.8×10^{20}	561	561
696-17	Zr-2	2.02×10^{13}	1.5×10^{20}	561	561
696-18	Zr-2 + 1Nb	2.02×10^{13}	4.6×10^{20}	616	616
696-19	Zr-2	2.46×10^{13}	4.6×10^{20}	616	616
696-20	Zr-2	2.46×10^{13}	1.8×10^{20}	616	616
696-21	Zr-2 + 1Nb	2.37×10^{13}	5.0×10^{20}	616	294
696-22	Zr-2	2.46×10^{13}	5.0×10^{20}	616	294
696-23	Zr-2 + 1Nb	2.61×10^{13}	1.9×10^{20}	616	616
696-24	Zr-2 + 1Nb	2.71×10^{13}	3.6×10^{20}	561	294
696-25	Zr-2	2.70×10^{13}	3.6×10^{20}	561	294
696-26	Zr-2 + 1Nb	2.66×10^{13}	1.3×10^{20}	561	561

Table 4
Minimum creep rate achieved for each set of test conditions.

ID	Set	Temp. (K)	Applied stress (MPa)	Fluence (n/cm^2)	Minimum strain rate (1/s)	Achieved steady state
696-1	1	562	138	2.11×10^{20}	1.9×10^{-10}	No
696-1	2	564	310	2.93×10^{20}	2.2×10^{-9}	No
696-1	3	569	352	3.07×10^{20}	7.4×10^{-9}	Yes
696-2	1	562	241	2.17×10^{20}	1.7×10^{-10}	No
696-2	2	563	365	2.97×10^{20}	7.9×10^{-10}	No
696-2	3	563	400	3.34×10^{20}	3.0×10^{-10}	No
696-2	4	563	427	3.76×10^{20}	3.4×10^{-10}	No
696-3	1	559	241	2.13×10^{20}	5.5×10^{-10}	No
696-3	2	567	331	3.34×10^{20}	2.3×10^{-9}	No
696-4	1	620	138	2.17×10^{20}	2.9×10^{-10}	No
696-4	2	621	276	3.37×10^{20}	4.2×10^{-10}	No
696-5	1	619	172	2.66×10^{20}	2.2×10^{-10}	No
696-5	2	621	310	4.04×10^{20}	3.9×10^{-10}	No
696-5	3	623	372	4.54×10^{20}	1.0×10^{-9}	No
696-6	1	619	69	2.65×10^{20}	1.1×10^{-10}	No
696-6	2	620	248	4.03×10^{20}	1.8×10^{-9}	No
696-6	3	620	303	4.48×10^{20}	2.1×10^{-7}	Yes
696-7	1	617	172	2.52×10^{20}	4.8×10^{-10}	No
696-8	1	618	103	2.65×10^{20}	1.7×10^{-10}	No
696-8	2	617	331	4.03×10^{20}	4.9×10^{-10}	No
696-8	3	618	352	4.54×10^{20}	6.7×10^{-10}	No
696-9	1	618	103	2.69×10^{20}	2.0×10^{-10}	No
696-10	1	561	172	2.80×10^{20}	1.9×10^{-10}	No
696-10	2	620	172	4.33×10^{20}	4.3×10^{-10}	No
696-10	3	621	290	4.81×10^{20}	5.3×10^{-8}	Yes
696-14	1	560	172	2.83×10^{20}	1.2×10^{-10}	No
696-14	2	564	400	4.36×10^{20}	3.2×10^{-10}	No
696-14	3	564	455	4.91×10^{20}	1.8×10^{-9}	No
696-12	1	563	172	2.85×10^{20}	1.9×10^{-10}	No
696-12	2	568	372	3.89×10^{20}	7.1×10^{-8}	Yes

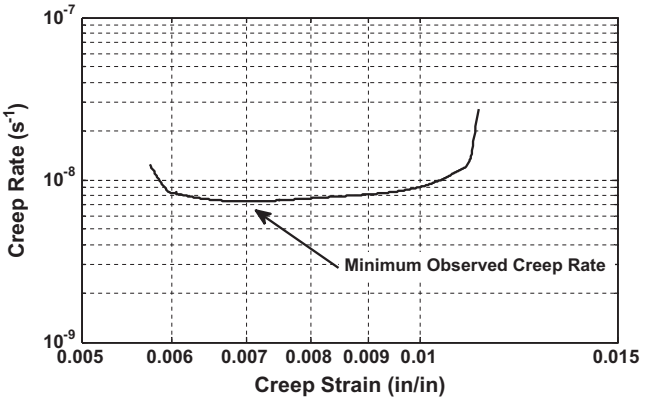

Fig. 3. Creep strain-rate vs. creep strain for Specimen 696-1 at an applied stress of 352 MPa, plotted on logarithmic axes.

days to resume the pre-shutdown creep behavior. This shutdown was different from all other shutdowns in two ways. First, it was 3293 h (137 days) in duration, 2899 h (120 days) longer than the second longest shutdown. More notably, this "shutdown" included an unplanned 21-day period during which the reactor had a fast neutron flux between 1×10^{13} n/cm^2 s and 2×10^{13} n/cm^2 s and a temperature between 520 K and 560 K, with no applied stress (no pressure on the bellows). All twelve (12) creep specimens in this test program experienced this unplanned stress step-change to zero stress. Fig. 5 plots the change in strain for Specimen 696-2 during this 21-day stress-free irradiation period.

During all other shutdowns lasting longer than a few hours, specimens were out-of-flux and at temperature less than 366 K. After these events, the creep rate returned to the previous creep rate within a matter of hours following reactor startup.

4.3. Tensile testing

A summary of out-of-reactor post-irradiated tensile testing results for the 12 specimens that were irradiated stress-free are included in Table 5. As part of the pre-irradiation certification of the materials irradiated in the HALDEN Reactor, tensile testing of non-irradiated Zircaloy-2 and Zircaloy-2 + 1 wt% Nb was conducted at room-temperature, 561 K and 616 K. These test results are also included in Table 5.

Prompt necking after yielding occurred for all post-irradiated Zircaloy-2 specimens, but did not occur for post-irradiated Zircaloy-2 + 1 wt% Nb specimens. A comparison of typical stress–strain curves for post-irradiated Zircaloy-2 and Zircaloy-2 + 1 wt% Nb specimens is included as Fig. 6.

5. Discussion

5.1. Steady-state creep

Steady-state creep rate is one of the most common metrics of a material's creep strength. Many empirical and phenomenological models have been used to describe in-pile creep of Zircaloy [8–25]. Most of these models focus on a limited stress regime, most commonly the low stress regime where creep rate is generally taken to be nearly linearly dependent upon applied stress. Four of the more general models that attempted to describe creep behavior over a broad range of test conditions are studied here. These models are MATPRO [10,11], a model by Watkins et al. [12], a model by Limbäck et al. [13], and a model by Nichols [14].

MATPRO relates in-reactor creep rate to time (t) in seconds according to

$$\dot{\varepsilon} = K\phi[\sigma + B \times exp(C\sigma)] \times \exp(-Q/RT_K) \times t^{-1/2} \quad (1)$$

where $\dot{\varepsilon}$ is steady-state creep rate (s^{-1}), σ is applied stress (Pa), ϕ is fast neutron flux (n/cm^2 s), T_K is absolute temperature (K), Q is an

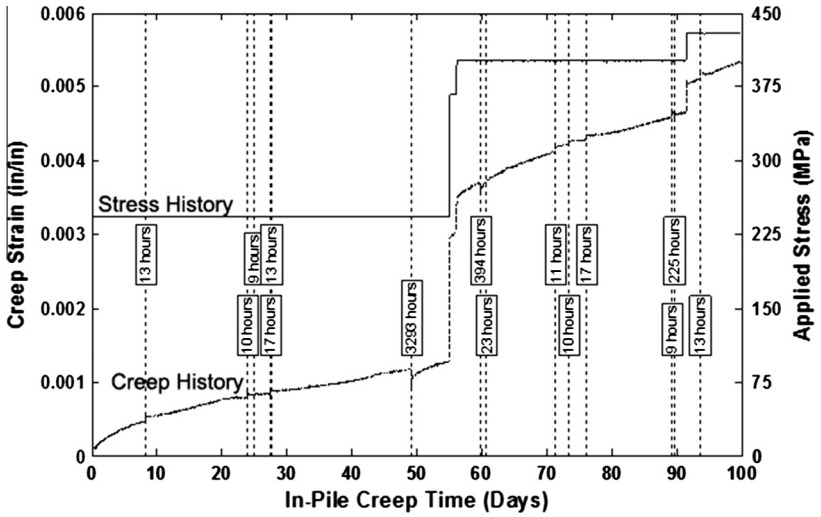

Fig. 4. Applied stress and creep strain vs. in-pile time for Specimen 696-2, tested at a nominal temperature of 561 K. Periods of reactor shutdown are indicated in hours.

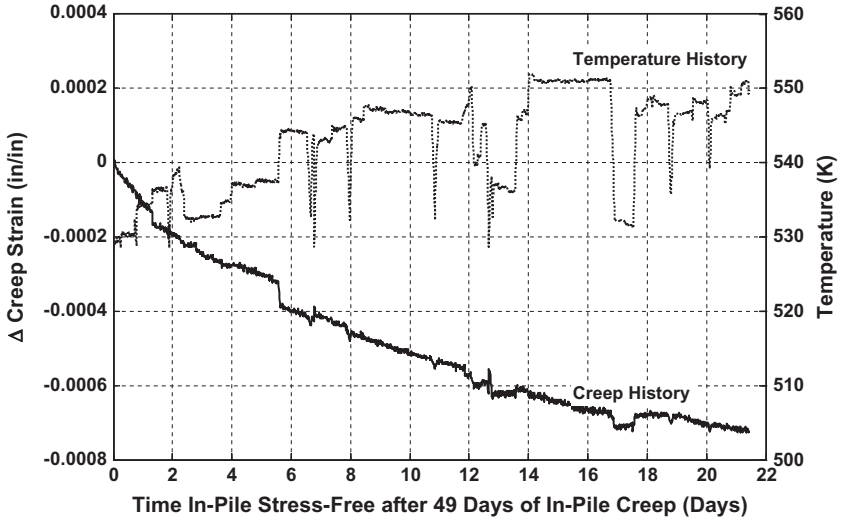

Fig. 5. Creep contraction observed for Specimen 696-2 during 21-day stress-free irradiation period following 49 days of stressed in-pile creep.

activation energy with a literature value of 10,000 cal/mol [11], R (=1.987 cal/mol K) is the universal gas constant, and K (=5.129×10^{-29}), B (=7.252×10^{2}), and C (=4.967×10^{-8}) are constants with values taken from the literature for longitudinal Zircaloy-4 [11]. Fig. 7 compares predictions of MATPRO to the HALDEN in-pile creep results for Zircaloy-2 tested at 616 K. Experimental data can be predicted accurately by Eq. (1) at a snapshot in time, although values of parameters K, B, and C would need to be adjusted to correct the time scale. Even so, the time required to achieve the minimum creep rate is a strong function of applied stress and minimum creep rate could be more accurately generalized to occur at a consistent magnitude of plastic strain, rather than after a given period of time. Fig. 7 also includes predictions of MATPRO calculated at a constant magnitude of plastic strain. Since $\dot{\varepsilon} \propto t^{-1/2}$, at lower creep rates it takes a very long time to accumulate a given amount of strain. MATPRO can accurately predict creep behavior over a wide range of stresses at a snapshot in time, but it is not an ideal general model to describe strain-rate vs. strain data.

Watkins et al. [12] predicted in-reactor creep rates using a hyperbolic sine function

$$\dot{\varepsilon} = 1.02 \times 10^{-11} \phi^{0.85} \times \sinh(1.15 \times 10^{-4} \sigma) \times \exp(-Q/RT_K) \quad (2)$$

where Q has a value of 14,000 cal/mol [12]. By employing a hyperbolic sine function, Eq. (2) accurately models in-reactor creep results in the low-stress and intermediate-stress regimes, but Eq. (2) under-predicts the stress-dependence of in-reactor creep at the highest applied stresses (see Fig. 7). Since Watkins et al. [12] did not study creep behavior in the high-stress regime, it would not be expected that Eq. (2) describes creep behavior in the high-stress regime.

Limbäck et al. [13] expressed creep as the sum of a linear in-reactor creep rate at low stresses and a hyperbolic sine dependence of in-reactor creep rate at higher-stresses:

$$\dot{\varepsilon} = \dot{\varepsilon}_{ir} + \dot{\varepsilon}_{th} \quad (3)$$

where

$$\dot{\varepsilon}_{ir} = C(1 \times 10^{4} \phi)^{c_1} \times \sigma^{c_2} \quad (4)$$

$$\dot{\varepsilon}_{th} = A(E/T_K) \times [\sinh(a\sigma/E)]^{n} \times exp(-Q/RT_K) \quad (5)$$

Table 5
Summary of non-irradiated and post-irradiation tensile tests.

ID	Fluence (n/cm^2)	Irradiation temp. (K)	Test temp. (K)	YS (MPa)	UTS (MPa)	UE (%)	TE (%)
Zircaloy-2 Specimens							
Ref-01	0	n/a	294	407	542	13.3	24.2
Ref-02	0	n/a	294	405	552	13.1	22.1
Ref-03	0	n/a	561	154	247	12.0	41.7
Ref-04	0	n/a	561	154	252	14.3	39.6
Ref-05	0	n/a	616	133	216	21.3	47.7
Ref-06	0	n/a	616	125	219	16.5	47.9
696-17	1.5×10^{20}	561	561	434	434	0.2	3.5
696-20	1.8×10^{20}	616	616	458	458	0.2	2.2
696-25	3.6×10^{20}	561	294	761	761	0.2	1.7
696-22	5.0×10^{20}	616	294	799	799	0.2	1.4
696-15	3.8×10^{20}	561	561	481	481	0.2	2.1
696-19	4.6×10^{20}	616	616	481	481	0.2	2.0
Zircaloy-2+1%Nb Specimens							
Ref-07	0	n/a	294	435	569	11.3	26.1
Ref-08	0	n/a	294	427	576	12.7	27.9
Ref-09	0	n/a	561	164	256	14.1	44.5
Ref-10	0	n/a	561	173	265	11.6	43.8
Ref-11	0	n/a	616	141	230	13.2	43.3
Ref-12	0	n/a	616	145	230	15.3	52.4
696-26	1.3×10^{20}	561	561	440	469	2.8	5.5
696-23	1.9×10^{20}	616	616	451	467	2.2	4.1
696-24	3.6×10^{20}	561	294	709	751	2.6	5.2
696-21	5.0×10^{20}	616	294	785	809	1.7	2.9
696-16	3.8×10^{20}	561	561	540	540	0.2	3.2
696-18	4.6×10^{20}	616	616	547	547	0.5	2.4

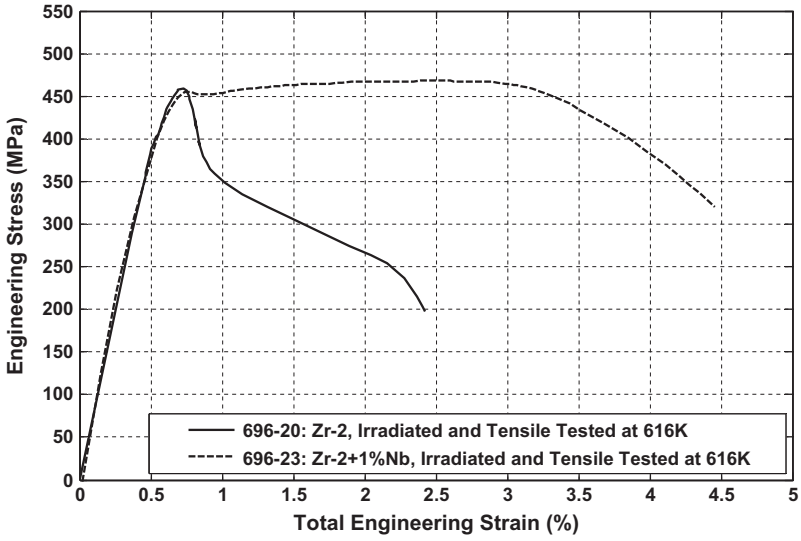

Fig. 6. Engineering stress–strain curves for Zircaloy-2 and Zircaloy-2 + 1 wt% Nb irradiated and tested at 616 K.

$$a = a_1\{1 - a_2[1 - exp(-a_3(\phi t)^{a_4})]\} \quad (6)$$

c_1 (=0.85), c_2 (=1), n (=3.5), E (=1.1585 × 10^5 − 59.9 T_K MPa), Q (=48,000 cal/mol), a_1 (=650), a_2 (=0.56), a_3 (=1.47 × 10^{27}), and a_4 (=1.3) are constants given by [13] and values of A and C were adjusted to fit the current experimental data. Similar to Eqs. (2) and (3) accurately models the present in-reactor creep results in the low-stress and intermediate-stress regimes, but under-predicts the stress-dependence of in-reactor creep at the highest applied stresses (see Fig. 7). Also similar to [12], Ref. [13] did not study creep behavior in the high-stress regime, so it would not be expected that Eq. (3) describes creep behavior in the high-stress regime. Both Eqs. (2) and (3) would provide a good description of the present data if updated to include a description of creep behavior in the high-stress regime.

Nichols [14] put forth a theory of in-pile creep for Zircaloy stating that in-pile creep can be divided into three stress regimes: low, intermediate, and high. At low stresses, irradiation induced creep was taken to be linearly dependent upon fast neutron fluence and applied stress following Ross-Ross et al. [15]. In [14], Nichols removed the temperature dependence from the equation in [15], limiting the application of the model to a single temperature. Due to the multiple test temperatures in the current work, the temperature dependent irradiation induced creep model from [15] was assumed of the form

$$\dot{\varepsilon}_1 = [B\phi(T_K - 433)] \times \sigma \quad (7)$$

where $\dot{\varepsilon}_1$ is steady-state creep rate (s^{-1}) and B (cm^2/(n K Pa)) is a constant specific to a material system and was adjusted to fit the experimental data (see Table 6).

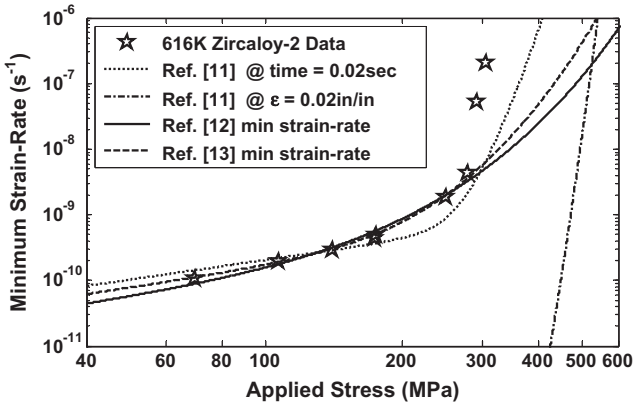

Fig. 7. MATPRO [11], a model by Watkins et al. [12], and a model by Limbäck et al. [13] compared to present data.

At intermediate stresses [14] assumed that irradiation damage has a similar impact on creep strength compared to dispersion hardening. A creep model with a linear dependence on flux and a stress exponent of four was adopted based on Ansell et al. [16]. As with the previous equation [14] removed the temperature dependence from the equation in [16]. Combining temperature independent constants into a single term (C_1), the model in [16] can be expressed as

$$\dot{\varepsilon}_2 = [C_1 \phi exp(-Q/RT_K)/\mu^3 kT_K] \times \sigma^4 \quad (8)$$

where μ is shear modulus (Pa) and k is Boltzmanns' constant (J/K). Parameters C_1 ((cm^2 J)/(n Pa)) and Q (cal/mol) are constants specific to a material system and were adjusted to fit the experimental data (see Table 6).

At high stresses, deformation becomes too rapid for fast neutron flux to affect creep rates and the in-pile creep strength was taken to be equivalent to the out-of-pile post-irradiated creep strength. A specific post-irradiation creep equation was not identified in [14]. In the current work, a simple empirical hyperbolic sine model based on the modified jogged-screw dislocation model [17,18] was employed to describe deformation at high stresses of the form

$$\dot{\varepsilon}_3 = [D_1 exp(-Q_{th}/RT_K)] \times \sinh(D_2 \sigma/\mu) \quad (9)$$

where Q_{th} is an activation energy (cal/mol), D_1 is a constant (s^{-1}), and D_2 was taken to be a constant in the present work due to the narrow range of fluences studied, but is more generally a function of fluence. Values for D_1, D_2, and Q_{th} were adjusted to fit the experimental data. Parameter values that were assumed in this work for Eqs. (7)–(9) are summarized in Table 6. The value for μ was based on [19].

Neglecting stress-free growth [14] then takes the total creep rate to be

$$\dot{\varepsilon} = \dot{\varepsilon}_1 + 1/[1/\dot{\varepsilon}_{int} + 1/(\dot{\varepsilon}_2 + \dot{\varepsilon}_3)] \quad (10)$$

where $\dot{\varepsilon}_{int}$ represents the intrinsic non-irradiated creep rate of the alloy. When $\dot{\varepsilon}_{int}$ is taken to be much greater than $\dot{\varepsilon}_1$, $\dot{\varepsilon}_2$, and $\dot{\varepsilon}_3$, Eq. (10) reduces to

$$\dot{\varepsilon} = \dot{\varepsilon}_1 + \dot{\varepsilon}_2 + \dot{\varepsilon}_3 \quad (11)$$

Fig. 8 compares model predictions of Eq. (11) to the nominal 616 K Zircaloy-2 experimental data irradiated to fluences ranging from 2×10^{20} n/cm^2 to 5×10^{20} n/cm^2 from Table 4. The creep rates predicted by Eqs. (7), (8), (9), (11) are included in Fig. 8. Note that although there are three discrete equations with different stress exponents, the effective stress exponent increases smoothly with applied stress. The lowest stress data falls above model predictions because minimum creep rates were not achieved.

Fig. 9 plots Eq. (11) against all experimental creep data in Table 4. Eq. (7) parameter values were set based on the assumption that creep at lower stresses was insensitive to the Nb addition. This is a reasonable assumption, but cannot be conclusively proven based on the current data since minimum creep rates were not obtained. At higher stresses, the data clearly demonstrate that the 1 wt% Nb addition increased creep strength. This is presumably because niobium impedes dislocation motion by way of solid solution strengthening and the presence of Zr–Nb precipitates, although electron microscopy confirmation of these hypotheses are not available at this time.

5.2. Primary creep

The most unique feature of creep testing in the HALDEN Reactor is the ability to in situ monitor primary creep behavior at the beginning of testing and the transitional period of evolving creep rate following a step change to different test conditions. This transitional period following a step change is most likely attributable to either dislocation-based primary creep or irradiation assisted diffusion-based transient creep. Primary creep is attributed to strain-hardening in the microstructure associated with dislocation network evolution and can occur either with or without irradiation. Transient creep results from the irradiation assisted movement of interstitials and vacancies to relieve internal stresses, and as such it only occurs under irradiation [28].

Both of these mechanisms evolve toward characteristic steady-state behavior associated with a given set of test conditions. The duration of primary creep is dependent upon the strain increment required to re-equilibrate the dislocation substructures, whereas [28–32] show that the duration of the transient creep is dependent upon time. Following is a calculation of the expected in-pile time for the irradiation assisted transient creep to reach steady-state behavior assuming the conditions in the HALDEN Reactor.

The coupled set of differential equations for mobile point defects, as developed by Sizmann [30] and Lam [31], were solved with and without spatial dependence for irradiation conditions similar to that of the HALDEN Reactor [32]. It was shown that at a temperature of 600 K and a fast neutron flux of 1×10^{13} n/

Table 6
Parameter values for Eqs. (7)–(9).

Equation	Parameter	Zr-2	Zr-2+1%Nb	Units
(7)	B	1.6×10^{-30}	1.6×10^{-30}	cm^2/(n K Pa)
(8)	C_1	3.6×10^{-40}	1.3×10^{-41}	(cm^2 J)/(n Pa)
(8)	Q	14,000	14,000	cal/mol
(8)	μ	4.252×10^{10}–$2.218 \times 10^{7} \cdot T_K$	4.252×10^{10}–$2.218 \times 10^{7} \cdot T_K$	Pa
(8) and (9)	R	1.987	1.987	cal/(mol K)
(8)	k	1.38×10^{-23}	1.38×10^{-23}	J/K
(9)	D_1	3.0×10^{5}	3.0×10^{5}	s^{-1}
(9)	Q_{th}	85820	85820	cal/mol
(9)	D_2	4.0×10^{3}	2.9×10^{3}	–

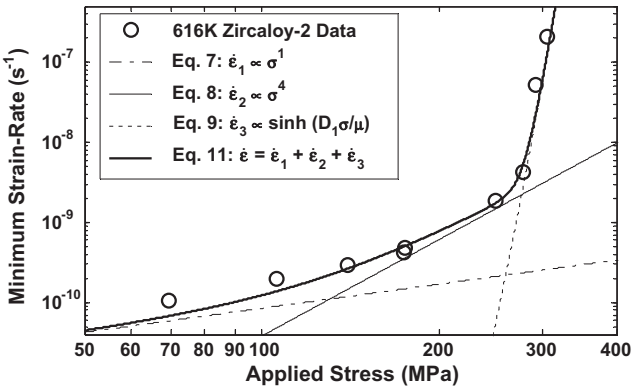

Fig. 8. Creep rates predicted by Eqs. (7), (8), (9), (11), compared to experimental data specimens irradiated to fluences ranging from 2×10^{20} n/cm^2 to 5×10^{20} n/cm^2.

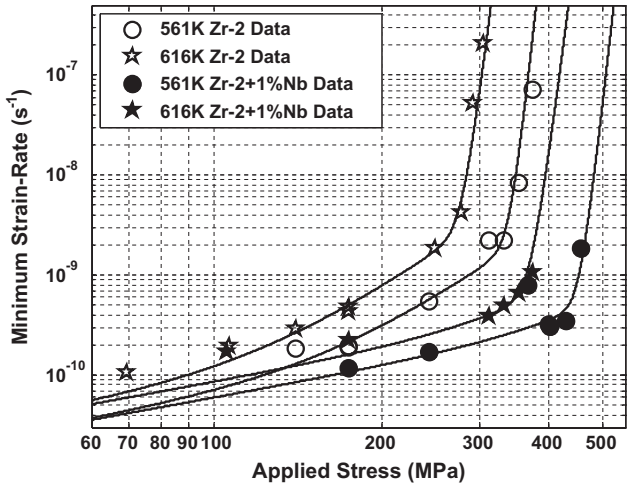

Fig. 9. Creep rates predicted by Eq. (11) compared to all experimental data in Table 4.

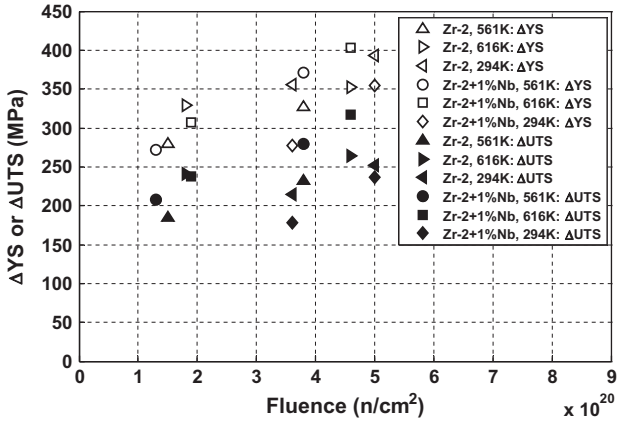

Fig. 10. Post-irradiated ΔYS and ΔUTS relative to non-irradiated reference specimens from Table 5 as a function of fluence.

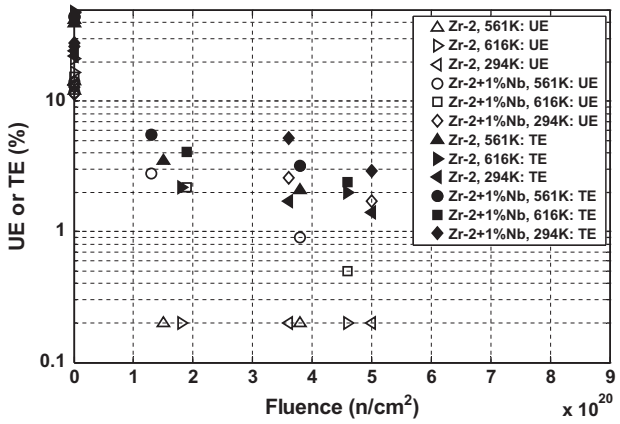

Fig. 11. Post-irradiated uniform elongation (UE) and total elongation (TE) as a function of fluence.

cm^2 s ($E > 1$ MeV) for Zircaloy material with relatively low dislocation density (10^{12} m^{-2}), the interstitial and vacancy concentrations reach their steady state values after a fluence increment of less than 10^{-6} DPA (6.6×10^{14} n/cm^2 ($E > 1$ MeV)). Interstitial and vacancy concentrations reach their equilibrium values more rapidly at greater dislocation density.

The calculations in Carter et al. [32] show that at the fast flux of the HALDEN Reactor (nominally 2×10^{13} n/cm^2 s ($E > 1$ MeV)) and for any dislocation density greater than 10^{12} m^{-2}, which is a reasonable lower limit of dislocation density for RXA Zircaloy-2, transient irradiation-induced creep behavior associated with point defect motion would reach steady-state in less than 100 s. This means that the gradual drop in creep rate occurring over a period of days as seen in Figs. 4 and 5 is more likely related to dislocation based evolution of the microstructure rather than motion of point defects.

After a step change to zero applied stress, all 12 creep specimens in this test program experienced creep contraction, with a decreasing contraction rate as a function of time (see Fig. 5). At the end of the 21-day in-pile non-stressed period, Specimen 696-2 had contracted by 0.0007 in./in. The implication is that the irradiation-hardened microstructure partially recovers, presumably by dislocation motion based on the above discussion, resulting in specimen contraction. Fig. 4 shows that upon further stressed in-pile creep at elevated temperature, a period of primary creep occurs before the creep response returns to the pre-shutdown creep rate after about 5 days. All 12 creep specimens had strain contractions of between 0.0005 in./in. and 0.0011 in./in. during the 21-day stress-free in-pile period in the "shutdown" at day 49.

5.3. Tensile testing

The specimens irradiated in the HALDEN Reactor demonstrated considerable increases in yield strength (ΔYS) and ultimate tensile strength (ΔUTS) relative to the non-irradiated specimens as seen in Fig. 10. At the highest irradiation exposures, about 5.0×10^{20} n/cm^2 ($E > 1$ MeV), yield strength increased by close to 400 MPa relative to the non-irradiated test results. The trend in the data suggests that at higher irradiation exposures, yield strength and ultimate tensile strength would be expected to continue to increase. Neither irradiation temperature, test temperature, nor the 1 wt% Nb addition had a significant impact on ΔYS as a function of fluence.

Uniform elongation (UE) and total elongation (TE) were significantly decreased relative to the non-irradiated specimens as seen in Fig. 11. The post-irradiated Zircaloy-2 specimens necked immediately upon yielding, but maintained some ductility as TE remained 1.4–3.5%. Necking at low plastic strain is common behavior for irradiated zirconium alloys and is a result of hardening due

to loop formation and dislocation channeling [26,27]. The post-irradiated Zircaloy-2 + 1 wt% Nb specimens experienced some strain-hardening prior to necking, having UEs ranging from 0.9% to 2.8%. The post-irradiated Zircaloy-2 + 1 wt% Nb specimens also had slightly higher TE compared to the Zircaloy-2 specimens without a Nb addition. The data suggest that at higher irradiation exposures, UE would continue to decrease for Zircaloy-2 + 1 wt% Nb and TE would continue to decrease for both Zircaloy-2 and Zircaloy-2 + 1 wt% Nb.

Fig. 6 shows prompt necking after yielding for a Zircaloy-2 specimen, but strain-hardening after yielding for a Zircaloy-2 + 1 wt% Nb specimen. This difference in behavior was consistent for all Zircaloy-2 and Zircaloy-2 + 1 wt% Nb tensile specimens. Without test data at higher fluences, it is uncertain if prompt necking after yielding due to dislocation channeling would occur in Zircaloy-2 + 1 wt% Nb materials irradiated to higher fluences.

6. Conclusions

In-pile in situ-monitored creep testing of two Zircaloy alloys was conducted, during which temperature and stress transients were independently applied to different specimens. The ability to monitor in situ creep rates following a stress change made possible the characterization of creep behavior over a wide stress–strain-rate–temperature design space for two variants of Zircaloy with only 12 test specimens in just a 100-day in-pile creep test program. This work corroborates Nichols [14] modeling efforts theorizing that during in-pile creep different deformation mechanisms are active in the low, intermediate, and high stress-regimes. In situ-monitoring also provided insight that at the stresses and temperatures investigated, the varying creep rate immediately following a stress transient is likely attributable to evolution of dislocation substructures rather than irradiation-assisted motion of point defects.

Zircaloy-2 specimens with a 1 wt% Nb addition had considerably greater in-pile creep strength at high stress conditions relative to Zircaloy-2 specimens without a Nb addition. Data suggests that at low stresses, when in-pile creep is taken to be linearly dependent on stress, the 1 wt% Nb addition has a negligible impact on creep strength. This could not be conclusively proven based on the current data since minimum creep rates were not obtained at the lowest applied stresses. Understanding the causes for the difference in creep strength between the Zircaloy-2 and Zircaloy-2 + 1 wt% Nb specimens would require metallographic and Transmission Electron Microscopy (TEM) examination of the irradiated microstructures. A test program is underway to characterize the microstructures of irradiated HALDEN specimens.

Acknowledgement

We would like to thank T. Karlsen of the OECD HALDEN Reactor Project for her efforts to make this test program a success.

References

[1] A. Nikulina, Metal Science and Heat Treatment 45 (7-8) (2003) 287.
[2] J. Foster et al., ZIRLO Material Composition and Fabrication Processing, European Patent Specification EP 0 475 159 B1, 1996.
[3] H. Chung, Nuclear Engineering and Technology 37 (4) (2005) 327.
[4] A. Rogozyanov et al., Journal of ASTM International 2 (3) (2005).
[5] D. Gilbon et al., in: G. Sabol, G. Moan (Eds.), Zirconium in the Nuclear Industry, ASTM STP 1354, 2000, p. 51.
[6] T. Karlsen, Private Communication, April 29, 2011.
[7] L. Greenwood et al., ANL/FPP/TM-197, January 1985.
[8] A. Soniak et al., in: E. Bradley, G. Sabol (Eds.), Zirconium in the Nuclear Industry, ASTM STP 1295, 1996.
[9] J. Gittus et al., Nuclear Applied Technologies 9 (1970) 40.
[10] C. Dixon, A Handbook of Materials Properties for Use in Light Water Reactor Fuel Rod Behavior, Idaho National Laboratory, TREE-NUREG-1005, 1976.
[11] D. Hagrman, NUREG/CR-6150, EGG-2720, vol. IV, 1993.
[12] B. Watkins et al., in: E. Baroch (Ed.), Application Related Phenomenon in Zirconium and its Alloys, ASTM STP 458, American Society for Testing and Materials, 1979, p. 370.
[13] M. Limbäck et al., in: E. Bradley, G. Sabol, (Eds.), Zirconium in the Nuclear Industry, ASTM STP 1295, American Society for Testing and Materials, 1996, p. 448.
[14] F. Nichols, Journal of Nuclear Materials 30 (1969) 249.
[15] P. Ross-Ross et al., Journal of Nuclear Materials 26 (1968) 2.
[16] G. Ansell et al., Transactions of the Metallurgical Society of AIME 215 (1959) 838.
[17] J. Moon et al., Journal of Nuclear Materials 353 (2006) 177.
[18] B. Morrow et al., Aca Materialia 61 (2013) 4452.
[19] C. Nam et al., Journal of Nuclear Materials 305 (2002) 70.
[20] E. Ibrahim, Journal of Nuclear Materials 46 (1974) 249.
[21] M. Andrews et al., Combustion Engineering Report CENPD-218, DOE, Contract EN-76-C-02-2426, 1976.
[22] D. Franklin, in: D. Franklin, R. Adamson (Eds.), Zirconium in the Nuclear Industry, ASTM STP 754, American Society for Testing and Materials, 1981, p. 235.
[23] Y. Lui et al., Energy Laboratory Report No. MIT-EL 77-012, 1977.
[24] S. Oldberg Jr., et al., in: J. Schemel, T. Papazoglou (Eds.), Zirconium in the Nuclear Industry, ASTM STP 681, American Society for Testing and Materials, 1979, p. 370.
[25] A. Miller, Unified Constitutive Equations for Creep and Plasticity, Elsevier, 1987.
[26] H. Rosenbaum et al., Metallurgical Transactions 5 (1974) 1867.
[27] T. Onchi et al., Journal of Nuclear Materials 88 (1980) 226.
[28] G. Was, Fundamentals of Radiation Materials Science, Springer, 2007.
[29] D. Olander, Fundamental Aspects of Nuclear Reactor Fuel, Elements, TID-26771-P1, 1976.
[30] R. Sizmann, Journal of Nuclear Materials 69–70 (1978) 386.
[31] N. Lam, Journal of Nuclear Materials 56 (1975) 125.
[32] J. Carter et al., Metallurgical and Materials Transactions A (2013) (submitted for publication).